

Article

Development of Synthesis Strategy of Ferric and Clayey Flat Ceramic Membranes

Rania Chihi¹, Antonio Comite² , Lamjed Mansour³ , Sana Hraiech⁴ and Fadhila Ayari^{1,*}

¹ Faculty of Sciences of Bizerte, LR 05/ES09 Laboratory of Applications of Chemistry to Resources and Natural Substances and to the Environment (LACReSNE), Carthage University, Zarzouna 7021, Tunisia

² Department of Chemistry and Industrial Chemistry, University of Genoa, Via Dodecaneso 31, 16146 Genoa, Italy

³ Department of Zoology, College of Science, King Saud University, P.O. Box 2455, Riyadh 11451, Saudi Arabia; lmansour@ksu.edu.sa

⁴ Physical Chemistry Laboratory of Mineral Materials and Their Applications, National Center of Researches in Materials Sciences, B.P.73, Soliman 8027, Tunisia; sana.hraiech@cnrsm.ucar.tn

* Correspondence: fadhila.ayari@ipeib.ucar.tn

Abstract: Ceramic membranes prepared with flat sheet configuration using local materials, iron ore and bentonite, are reported in this investigation. The feedstocks used were fully characterized using X-ray diffraction (XRD), thermogravimetric analysis (TGA), scanning electron microscopy coupled with energy dispersive spectroscopy (SEM-EDS) and laser diffraction/light scattering. In order to optimize the preparation conditions, the effect of sintering temperature on the microstructure of ferric and clayey membranes was assessed. Results obtained with SEM, confirmed by optical microscopy, indicate that the optimized sintering temperature was in the vicinity of 900 °C. The properties of the fabricated membranes were characterized in terms of mass and thickness loss throughout a determined period of time. The experimental results present a negligible variation in the rate of mass change, which suggested the stability of the synthesized membranes. Both the ferric and clayey membranes exhibit a prevalence of mesopores in their pore distribution. These results suggest that these specific membranes could be employed as cost-effective and environmentally friendly materials. Furthermore, they hold promise for potential applications in gas treatment processes.

Keywords: ceramic membranes; natural iron ore; bentonite; physico-chemical characterization; mesoporous membranes



Citation: Chihi, R.; Comite, A.; Mansour, L.; Hraiech, S.; Ayari, F. Development of Synthesis Strategy of Ferric and Clayey Flat Ceramic Membranes. *ChemEngineering* **2023**, *7*, 109. <https://doi.org/10.3390/chemengineering7060109>

Academic Editor: José P. Coelho

Received: 31 August 2023

Revised: 14 September 2023

Accepted: 16 October 2023

Published: 10 November 2023



Copyright: © 2023 by the authors. Licensee MDPI, Basel, Switzerland. This article is an open access article distributed under the terms and conditions of the Creative Commons Attribution (CC BY) license (<https://creativecommons.org/licenses/by/4.0/>).

1. Introduction

Over the last decades, membrane technologies have rapidly evolved and are considered reliable and technologically advanced processes for water treatment [1], the wastewater industry [2] and gas separation [3], protein separation [4] and other environmental applications. Ceramic membranes have received much more attention nowadays compared to polymeric membranes, which have specific properties due to their wide diversity of microstructures, porosities and accessible geometries [5–7].

Conventionally, alumina ($\alpha\text{-Al}_2\text{O}_3$ % \geq 99%) is considered the main body material for commercialized porous ceramic membranes. However, its use in full-scale applications is still limited to high capital costs, such as feedstocks (225.00 \$/kg) and the expensive cost of energy consumption in sintering (firing temperature up to 1500 °C). Furthermore, it is quite difficult to obtain a porous membrane with large pore size and good thermal shock resistance from alumina because of its high melting point (2050 °C) and high thermal expansion coefficient (theoretical value: $8.80 \times 10^{-6} \text{ }^\circ\text{C}^{-1}$ at 200–1000 °C).

To address large-scale application challenges, researchers have focused their interest in the fabrication and application of low-cost ceramic membranes based on naturally occurring raw materials and waste products (Table 1).

Table 1. Summary of different ceramic membranes.

References and Dates	Feedstocks and Configuration	Additives	Water Permeability	Porosity	Pore Size	Application
A. Dhivya et al., 2022 [8]	Ball clay and China clay Uniaxial pressing method	Quartz, calcium carbonate and polyvinyl alcohol	-	44–41%	1.18–0.31 μm	Suggested for microfiltration applications. Price: 924–1319/ m^2 (\$11.96–\$17.07)
J. H. Eom et al., 2015 [9]	Diatomite, kaolin and bentonite circular ceramic membranes	Talc, sodium borate and barium carbonate	-	34.6–36.3%	[0.29–0.67 μm]	Treatment of kerosene as an oily wastewater.
L. Hamoudi et al., 2023 [10]	Algerian clays, bentonite, aomar and kaolin Tubular support	Polyvinyl alcohol	Bentonite: 71.69 and 151.2 $\text{L m}^{-2} \text{h}^{-1} \text{bar}^{-1}$ Kaolin 547.37 $\text{L/m}^2 \text{h.bar}$	-	-	Clarification and retention of multiple pollutant loads of local cheese effluent.
M. Abbasi et al., 2010 [11]	Mullite and mullite–alumina	-	-	Mullite: 41% mullite–alumina: [44–56%]	Mullite: 0.3 μm mullite–alumina: 0.57 μm	Oil rejection was 93.8%.
R. Chihl et al., 2019 [12]	Bentonite ceramic tubular membranes	Amijel, methocel and starch	525 $\text{L h}^{-1} \text{m}^{-2} \text{bar}^{-1}$	-	1.7 μm	-
Q. Jiang et al., 2020 [13]	A SiC ceramic membrane using NaA(r) (and activated carbon powder)	Polypropylene and polyvinyl alcohol as an organic binder	3700 $\text{L m}^{-2} \text{h}^{-1} \text{bar}^{-1}$	46%	0.4 μm	Oil–water separation applications. Oil rejection was 93.8%.

The excellent properties of iron ore and bentonite (sodic smectite clay) have promoted us to develop innovative ceramic membranes. Both of them receive more attention by reasons of their high thermal and chemical stability, rugged structural and mechanical stability [14,15], environmental-friendliness, and abundance of availability as local materials, especially in Tunisia.

Considering those specific properties, iron ore and bentonite could be good candidates as feedstocks or as inorganic additives to create porous ceramic membranes and ensure good mechanical and chemical resistance.

Therefore, the current research focuses on an in-depth investigation of the development of novel ferric and clayey porous membranes for specific applications.

The properties of both raw materials used were fully characterized using X-ray diffraction (XRD), thermogravimetric analysis (TGA), scanning electron microscopy coupled with energy dispersive spectroscopy (SEM-EDS) and laser diffraction/light scattering. The determination of the optimal firing temperature was discussed by swiping the sintering temperature in order to optimize the preparation conditions. The properties of the fabricated membranes were characterized in terms of mass and thickness loss throughout a determined period of time. The surface texture of the membranes was observed and confirmed by using optical microscopy. Surface area measurements were employed to determine the pores distributions.

2. Materials and Methods

2.1. Raw Materials

The natural materials used to prepare ceramic membranes, iron and clay, were collected from an iron ore quarry situated in the Tamra region (northwest of Tunisia) and from Gabes (southeast of Tunisia), respectively.

The starting materials were dried after collection and crushed into small fragments, grounded into powder and sieved with 63 mesh.

The presence of additives within the ceramic paste is substantial. The low or high dose can influence plasticity and strength. The families of additives are chosen mainly according to their compatibility with an aqueous or non-aqueous medium.

Methocel was purchased from Dow Chemical Company. Amigel was purchased from Roquette Italia S. p. A. Starch and polyvinyl alcohol were purchased from RG 03408 Cerestar and Fluka 81384, respectively.

The solvent used for the preparation of a ceramic paste is water, which is the most commonly used for cost and safety reasons. The major disadvantage is during the drying process, where the evaporation rate compared to organic solvents seems to be lower.

2.2. Characterization of Materials

Different techniques were used to characterize raw materials and synthesized membranes. The phases presented in the powder composition were analyzed by an X-ray diffractometer using PanalyticalX'PertHighscore plus diffractometer with Cu K α radiation ($\lambda = 1.5406 \text{ \AA}$).

Particle size distribution measurements were conducted by employing Microtrac SYNC diffraction (measuring range: 0.01 μm –4 mm) correlated with the computer. Thermogravimetric analysis (TGA) was accomplished using a Mettler Toledo TGA/SDTA 851 apparatus with approximately 15 mg of samples heated from ambient to 900 °C at a constant rate of 5 °C/min under nitrogen.

Scanning electron microscopy (SEM) with a Hitachi S4800 was employed to examine the surface sample structure before and after the materials underwent sintering. The elemental composition was determined using EDX energy-dispersive X-ray microanalysis. Optical microscopy, in conjunction with a CCD camera, was utilized to observe the surface of both fabricated membranes (Dino-Lite AM4013MT5 model).

A thermal analysis was conducted to assess the microstructure of the produced membranes with the incorporation of organic additives and to estimate their impact on the properties of grain-to-grain connections. Two key parameters were monitored: mass loss and thickness. Over the course of three separate instances during an experimental period, measurements of weight and thickness were recorded at room temperature. These tests were carried out over a span of seven days. The textural characteristics of the samples were investigated by examining the adsorption and desorption isotherms of nitrogen at 77 K, utilizing a Quantachrome Nova 1200e surface and porosity analyzer. The mesopore volume distribution in relation to pore size was determined using the BJH (Barrett–Joyner–Halenda) method.

3. Materials Preparation

3.1. Shaping of the Ceramic Paste

In order to obtain a porous and resistant membrane, the addition of organic additives to the clay and/or iron ore-based raw material is necessary. Several tests have been carried out for the preparation of pastes with different types of additives with varying proportions of solvents. The powders are first mixed in order to obtain the best possible homogenization of both chemical compounds and mineral and organic additives. The organic parts are kept in the same order of introduction: the raw material first (clay or iron ore), followed by the binder, then the gelling agent, and lastly, the organic plasticizer. Thus, several series were prepared (Table 2). For the use of PVA, we resort to diluting this polymer in the solvent before adding it to the powder mixture.

Table 2. Chemical composition of clay and iron ore pastes for different tests used.

Samples	wt, %					
	Raw Material	Iron/Clay	Methocel	Amigel	Starch	PVA
Ferric membrane (1)	80	6	4	4	4	2
Clayey membrane (2)	86	-	6	4	4	-

Wet mixing was subsequently performed by introducing additional liquid solvent all at once, except when it was absolutely necessary to make adjustments due to the fact that both parameters (volume and mixing time) were independent of each other.

Once the paste is ready, two blocks will be presented: one will be adjusted and pressed in the form of pellets (diameter $1.3 \text{ cm} \pm 0.01$ and thickness $0.2 \text{ cm} \pm 0.01$). The second block will be left to rest in a humid atmosphere for two days.

The humidity is controlled during the drying time of the elaborated samples. The clayey and ferric pellets synthesized are presented in Figure 1.

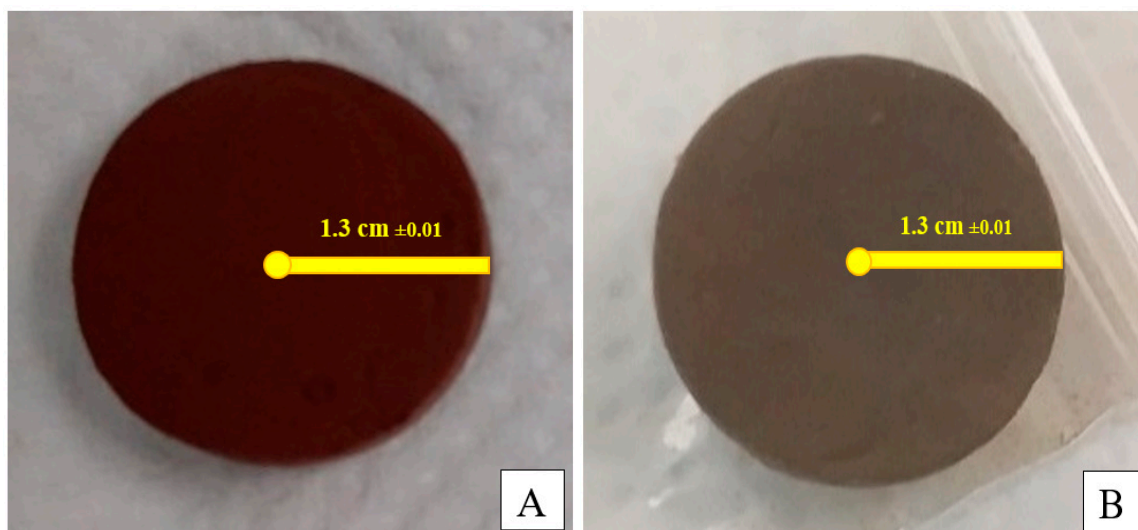


Figure 1. Images of synthesized membrane: ferric (A) and clayey (B).

3.2. Thermal Treatment

The composition of the powder and its granulometry are two parameters that intervene in the mode of firing. The use of gravimetric analysis allows us to understand the departure of the solvent, the degradation of the organic products and the chemical and structural transformations of the mineral materials [16].

The established program consists of steps of temperatures corresponding to these modifications in order to avoid the deterioration of the macroscopic structure of the ceramic by elimination or too fast transformation. Moreover, the temperature increases must allow the evacuation of combustion products of organic materials, volatile binders and water without staining the final product. The addition of mineral products, as is the case, influences the sintering quality and reduces the final firing temperature.

Before sintering the ceramic parts, the organic additives must be removed by a heat treatment at the lowest temperature. This step is very delicate as it can lead to many defects that affect the final structure of the part by forming cracks, blistering of the surface, and even bursting. For this purpose, a preliminary study by gravimetric analysis allows us to obtain indications of the degradation and the total elimination of the organic additives present during the firing.

The main specific parameters of this step are essentially the final firing temperature (T_f) and sintering time [17]. The setting thermal program is shown in Figure 2.

According to the thermal program, organic matter is destroyed with the elimination of hygroscopic water in a temperature range from 298 K to 523 K. A step of one hour is maintained to ensure the total disappearance of these elements. In order to avoid the appearance of microcracking during degassing, the heating rate is fixed at $2 \text{ }^\circ\text{C min}^{-1}$. For the second stage of two hours (between 250 $^\circ\text{C}$ and T_f), the heating rate is increased slightly ($5 \text{ }^\circ\text{C min}^{-1}$). This sintering lasts two hours; it is the sintering period.

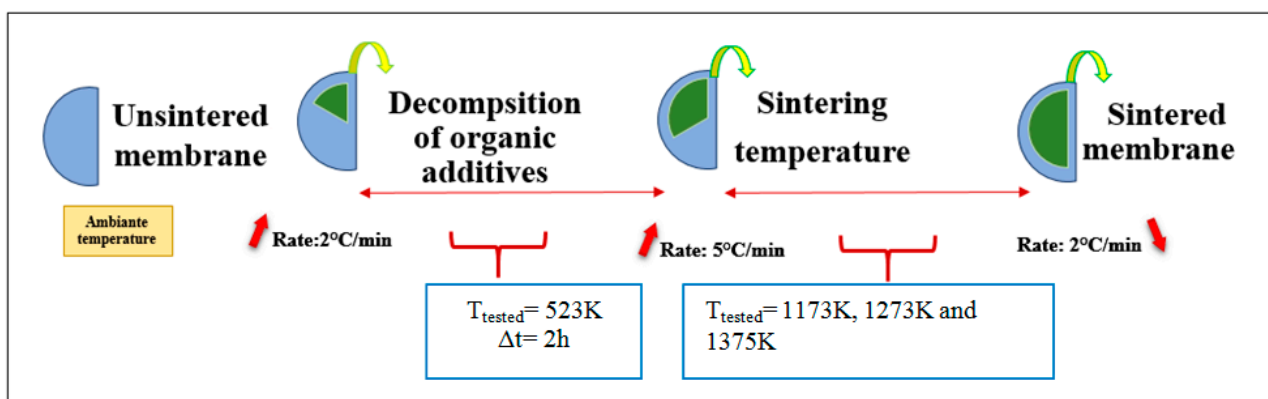


Figure 2. Temperature time sintering programs for the synthesis of iron and clay membranes.

4. Results and Discussion

4.1. Raw Materials Characterization

4.1.1. Mineralogical Analyses

Mineralogical analyses of starting powder materials at 25 °C were carried out by X-ray diffractometer (XRD) using a PANalytical X'Pert HighScore Plus diffractometer with CuK_{α} radiation ($\lambda = 1.5406 \text{ \AA}$).

Identification of the iron ore sample reveals the presence of the following phases: goethite $FeOOH$ ($2\theta = 21.2^{\circ}, 34.96^{\circ}, 36.8^{\circ}, 41.4^{\circ}, 50.5^{\circ}, 53.2^{\circ}$ and 59.3°) [18,19] and hematite Fe_2O_3 ($2\theta = 33.22^{\circ}, 40.5^{\circ}$ and 68.3°) [20]. In addition, a low amount of kaolinite can be clearly observed, with quartz as a minor phase (Figure 3).

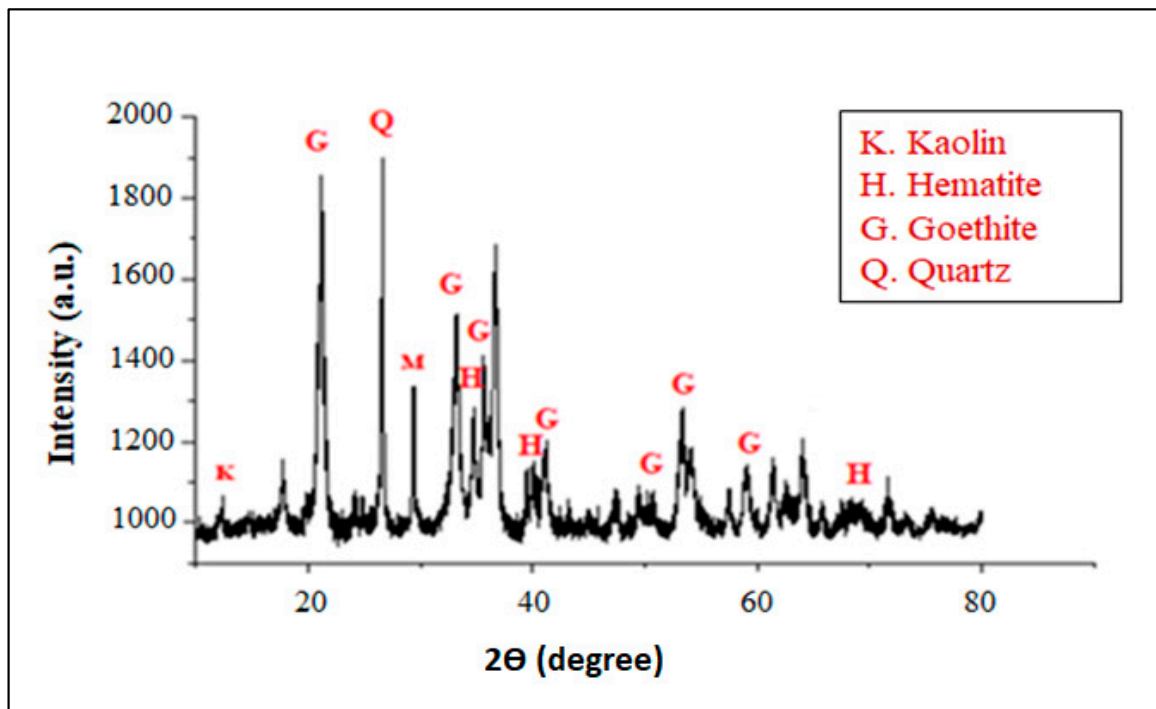


Figure 3. XRD pattern of iron ore as the starting material.

X-ray diffraction of clay suggests that it is a sodic smectite sample ($2\theta = 12.69^{\circ}$) associated with quartz ($2\theta = 20.89^{\circ}$ and 26.65°), calcite phases ($2\theta = 23.10^{\circ}, 26.65^{\circ}, 36.02^{\circ}$ and 39.45°) and kaolinite fraction ($2\theta = 12.38^{\circ}, 24.96^{\circ}$) (Figure 4) [21].

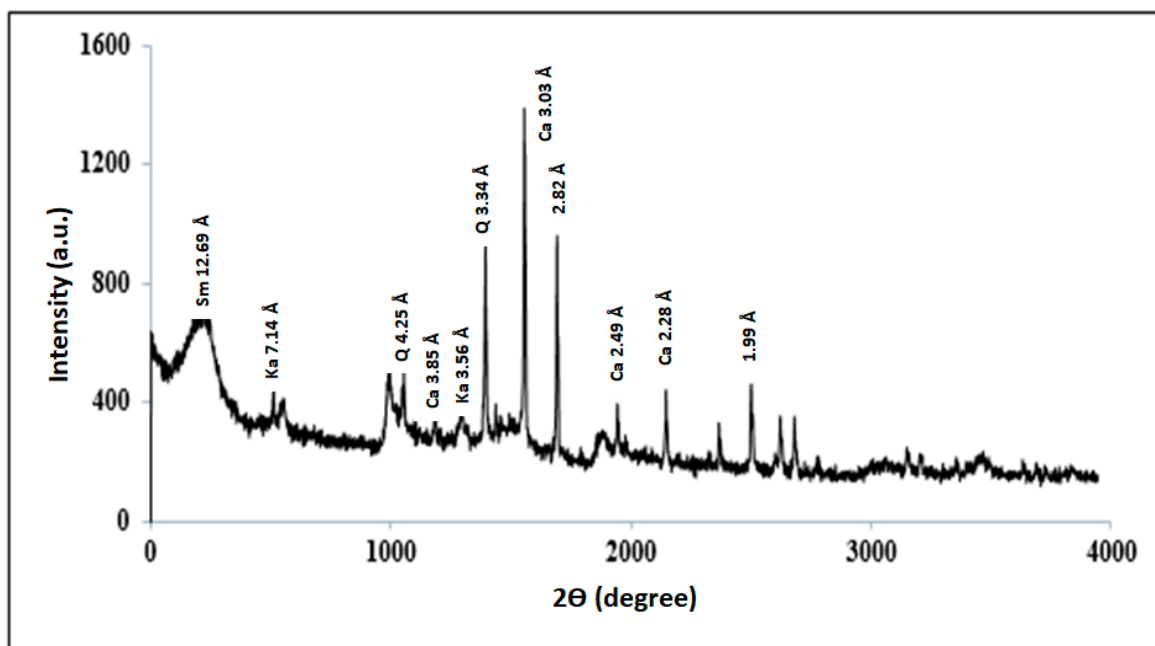


Figure 4. XRD pattern of the clay sample. (Sm = smectite, Ka = kaolinite, Q = quartz, Ca = calcite).

4.1.2. Thermogravimetric Analysis (TGA)

TGA of iron shows three mass loss steps. From 296 K to 423 K (Figure 5), a mass loss of 0.8% was attributed to a dehydration reaction. The second step (4.91%) occurs from the 473 K to 623 K temperature range assigned to the mineralogical transformation of goethite into hematite [21]. The third mass loss step (1.16%) is attributed to the loss of molecular oxygen corresponding to deshydroxylation that profoundly changes its structure and leads to metastable states evolving towards a stable state [22,23].

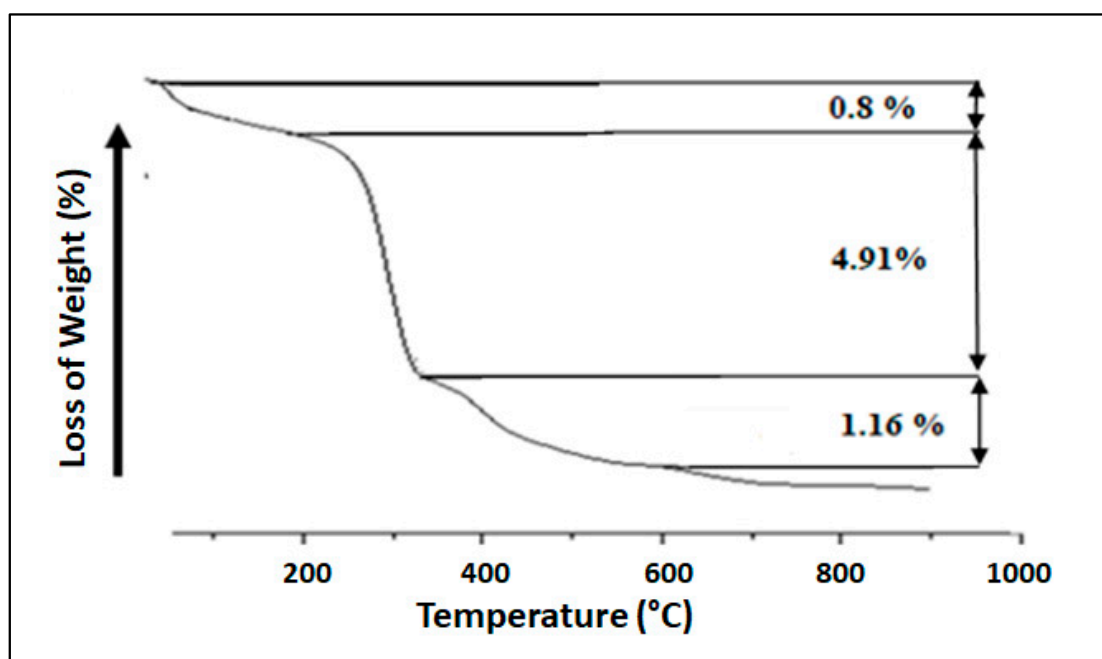


Figure 5. TGA thermogram of iron.

The thermal analysis curves of the clay, as shown in Figure 6, reveal three distinct reductions in mass. The initial mass reduction (10%), spanning from 323 K to 473 K, was

linked to the removal of moisture and water from interlayers (as depicted in Figure 6). The subsequent mass decline (3.08%) occurred within the temperature range of 473 K to 873 K and was associated with the loss of structural water. The final loss mass (8%) was attributed to the decarbonization of clay.

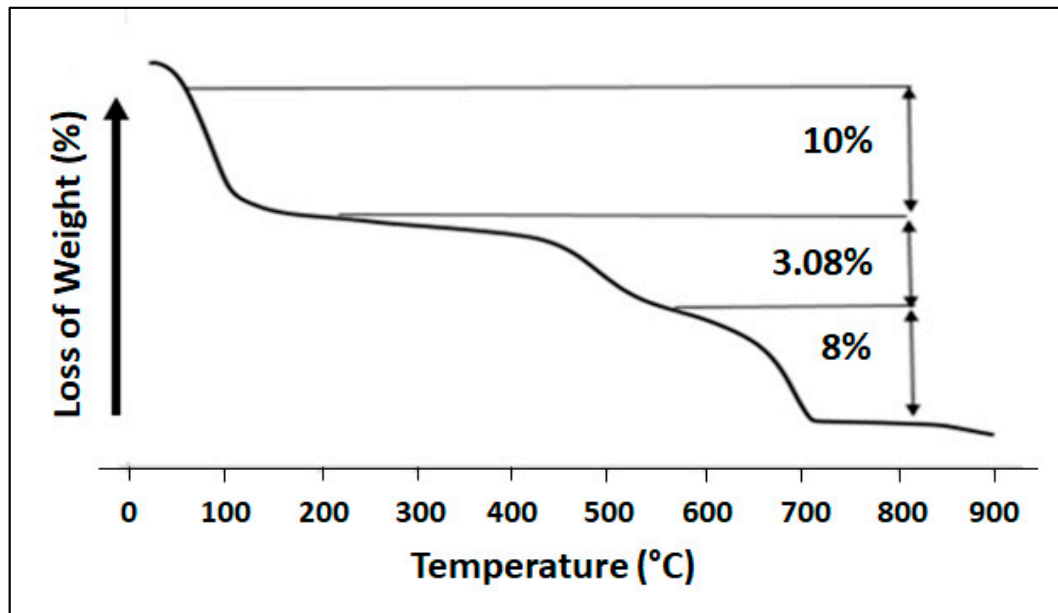


Figure 6. TGA thermogram of clay.

4.1.3. SEM Analyses

The SEM micrographs provide a broad overview of the surface morphology of the iron ore. The observations with a scanning electron microscope coupled to an EDX instrument (quantitative analysis), carried out on the iron ore, show the presence of aggregates of acicular and flat shape [24] and rhombohedral of heterogeneous dimension [25] (Figure 7). EDX shows that these platelets are composed of Fe, Si, Al, Mg, Na, Ca, Mn, Ti and O (Figure 8). These findings validate the outcomes obtained through X-ray diffraction (DRX) analysis, which also identifies the existence of these elements in oxide form: Al_2O_3 , SiO_2 , Fe_2O_3 , MgO , Na_2O , CaO and MnO et TiO_2 .

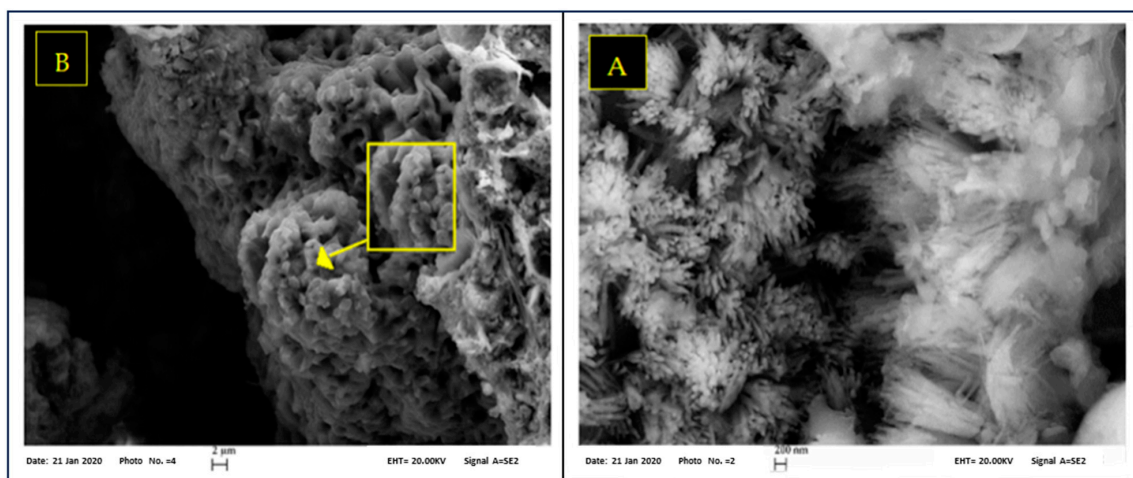


Figure 7. SEM micrographs of (A) hematite and (B) goethite powders [25].

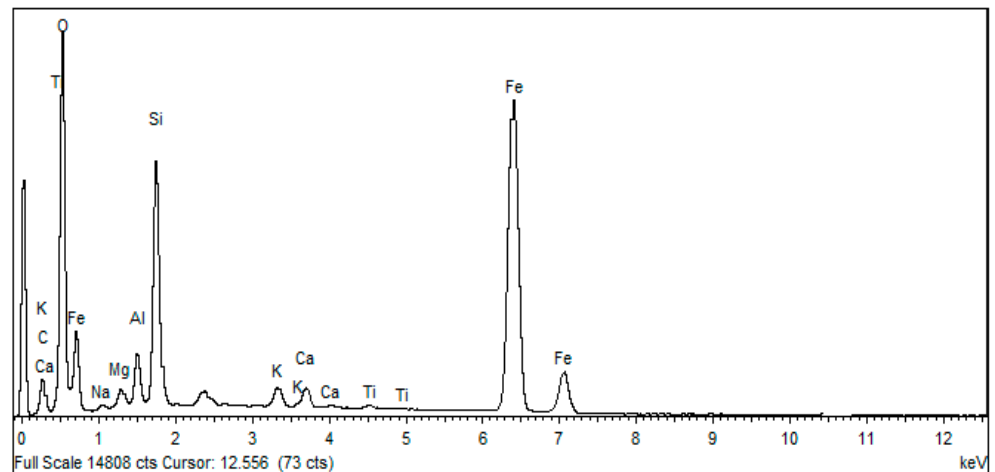


Figure 8. Raw iron ore EDX spectrum.

Bentonite SEM micrographs show the presence of spherical-shaped aggregates with heterogeneous dimensions (Figure 9). For a higher magnification (2 μm), large cavities of irregular shape are present. The EDX shows that these platelets are constituted of Al, Si, Mg, Fe, Na, Ca, K, Ti and O (Figure 10). These results confirm those found by the DRX and XRF analyses, which also reveal the presence of these elements in the form of oxides: Al_2O_3 , SiO_2 , Fe_2O_3 , MgO , Na_2O and K_2O et TiO_2 .

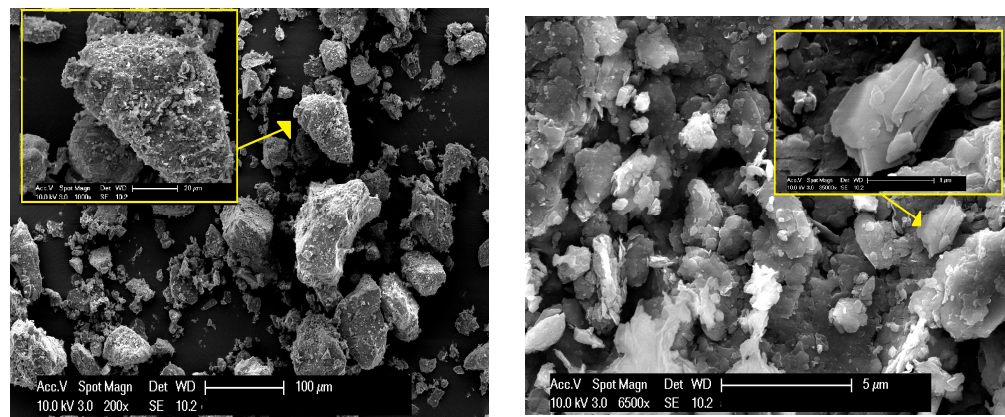


Figure 9. SEM micrographs of raw clay at different magnifications.

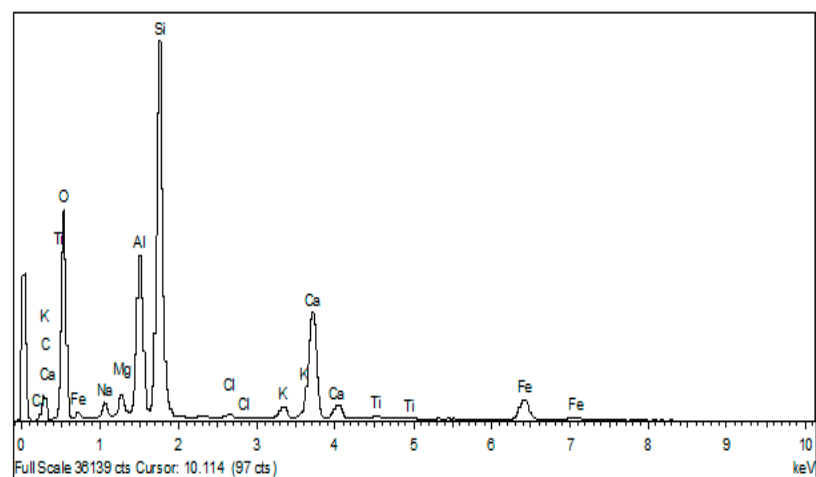


Figure 10. EDX spectrum of raw clay.

4.1.4. Particle Size Distribution Analyses

Particle size distribution measurement by laser diffraction/light scattering revealed that the shape of the particle size distribution is asymmetrical for both raw materials (Figures 11 and 12). It is worth noting that the majority of particle sizes are between 12 to 14 μm and 24 to 30 μm for iron and between 30 to 38 μm for clay. From these results, it can be inferred that iron, as well as clay, have a good finesse, which could have an effect on the compact density and porosity of the elaborated membranes.

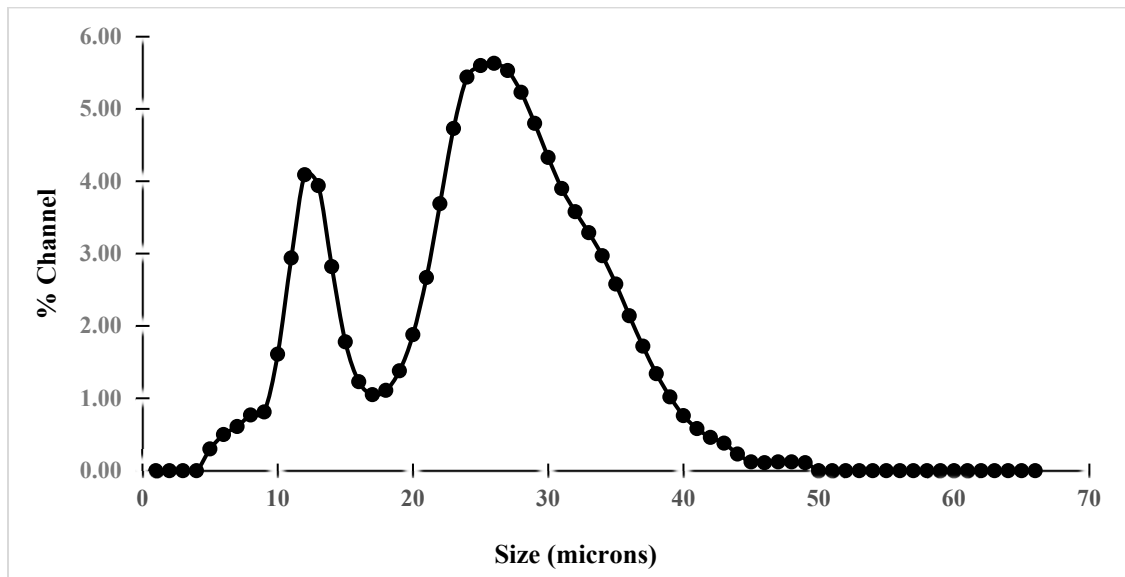


Figure 11. Particle size distribution of iron ore.

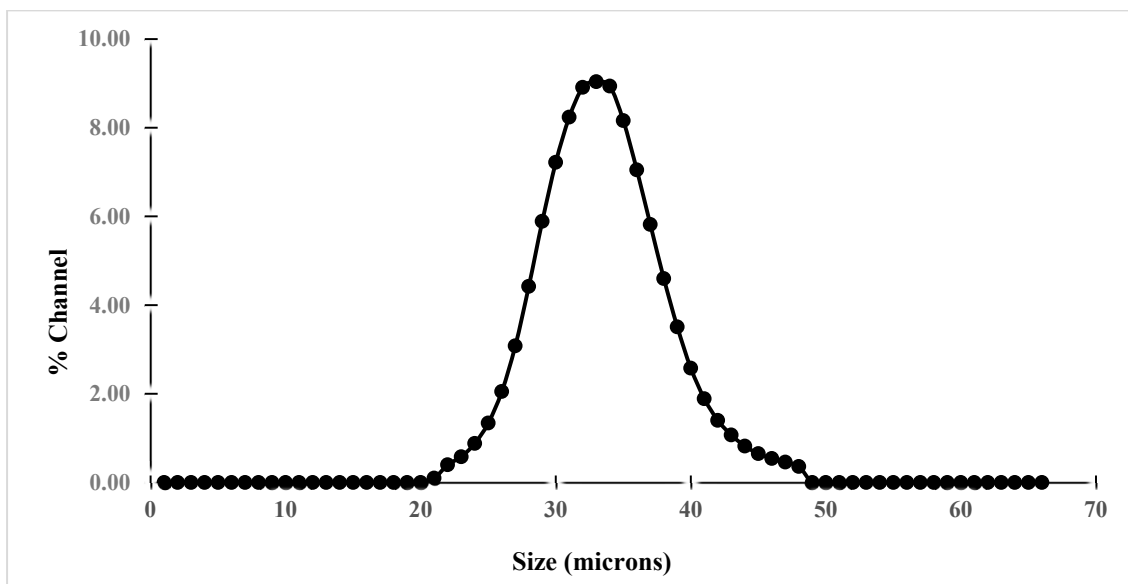


Figure 12. Particle size distribution of bentonite.

4.2. Characterization of the Membranes Elaborated

4.2.1. Study of Systematic Losses

The results (Figures 13 and 14) show that the variation of mass losses of ferric and clayey membranes does not exceed $0.02\% \pm 0.001$ during a journey, with or without aging. The same variation in thickness losses was evaluated to be $0.02\% \pm 0.001$.

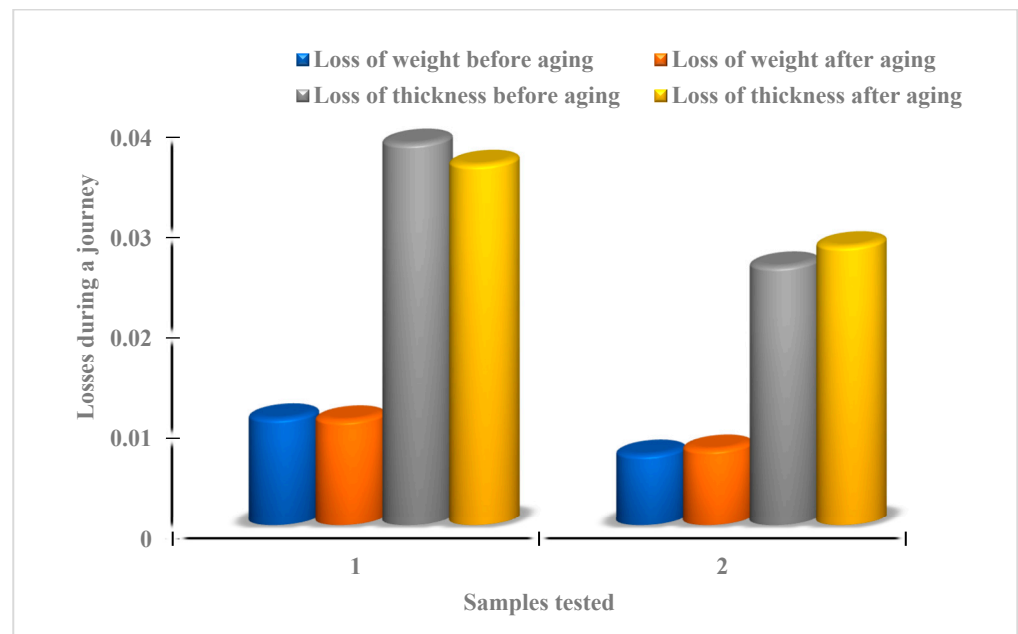


Figure 13. Summary of systematic losses of weight and thickness attributed to the ferric membrane (1) and clayey membrane (2) during a journey.

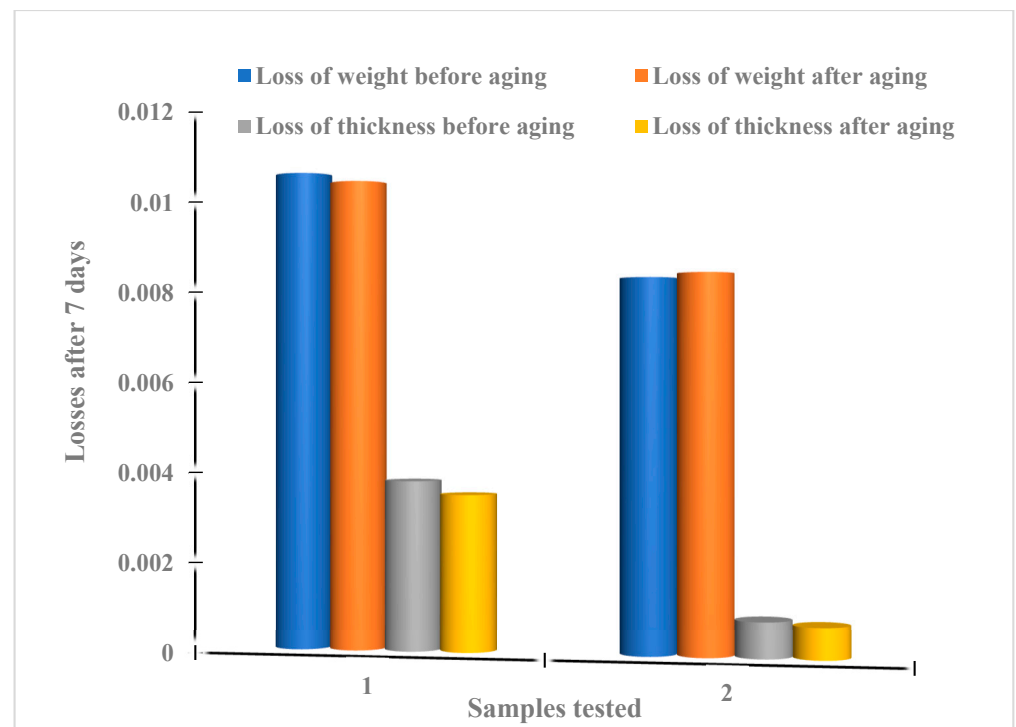


Figure 14. Summary of systematic losses of weight and thickness attributed to the ferric membrane (1) and clayey membrane (2) after 7 days.

Whatever the nature of the membranes present and the preparation conditions, with or without aging, the experimental results show a negligible variation in the rate of mass change (weight and/or thickness), suggesting the stability of the synthesized membranes (Table 3, Figures 13 and 14).

Table 3. Statistical description of losses with the variation of weight and thickness of clay and iron membranes during a journey.

	Clay's Membrane				Iron's Membrane			
Range	16.00				19.00			
Standard Deviation	4.00				4.35			
	Weight losses		Thickness losses		Weight losses		Thickness losses	
	Before Aging	After Aging	Before Aging	After Aging	Before Aging	After Aging	Before Aging	After Aging
Mean Absolute Deviation	4.35	4.24	4.95	4.68	4.95	4.68	5.01	4.72
Variance	24.89	24.12	32.62	29.22	32.62	29.22	33.48	29.82

4.2.2. SEM Analyses

The firing process starts to appear only after 1023 K, and the temperature at which the junction between grains begins and the solidification of the material is at a minimum. However, the internal reorganization of each grain is completed, and the dislocations align [25]. From 1073 K onwards, the contacts between grains continue to grow, allowing the pores to become spherical.

The results (Figures 15 and 16) show a consolidation between grains from 1073 K (clayey membrane); nevertheless, the corresponding mechanical resistance is weak. At 1173 K, the grains become sufficiently close, and the internal reorganization of each of them is well established, forming a strong roughness. At this stage, the presence of intergranular contacts can be detected, which is sufficient to ensure the cohesion of the ceramic. The beginning of the sintering process marks the end of the grain coarsening and the formation of the joints.

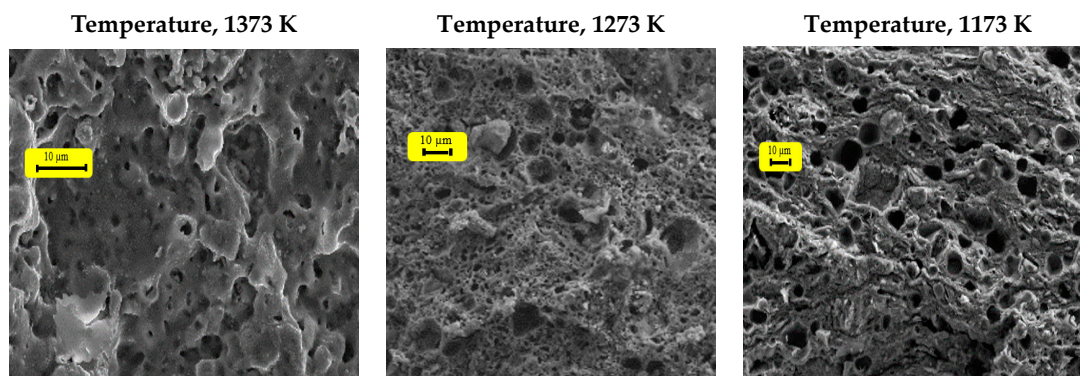


Figure 15. Pictures of clayey membranes, sieved at 60 μm , at different temperatures.

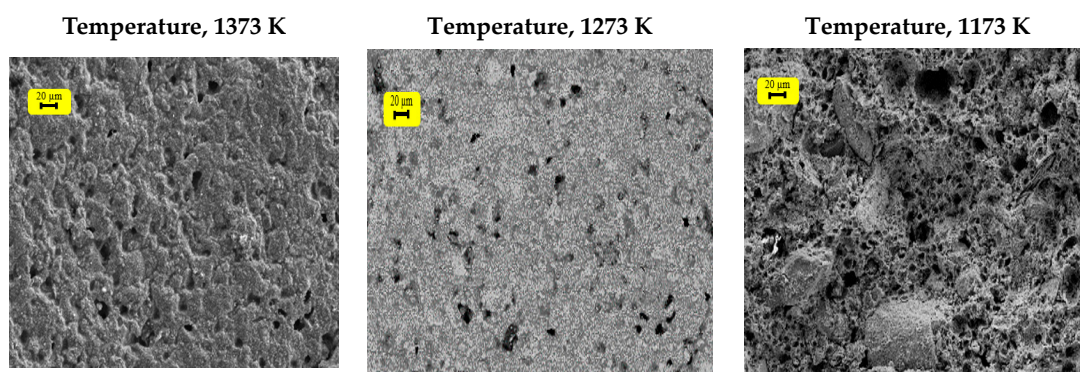


Figure 16. Pictures of ferric membranes, sieved at 60 μm , at different temperatures.

Beyond this, between 1273 and 1373 K, a phenomenon of densification appeared following the welding and the coarsening of the grains (Figures 15 and 16). The heat treatment at this stage leads to a more or less irregular growth of the particles. In fact, the small grains disappear to the benefit of larger ones. A tendency towards high temperatures is associated with the progressive elimination of porosity, which essentially leads to a totally monolithic membrane (solid block).

Therefore, the sintering temperature is fixed at 1173 K. The SEM pictures show the absence of agglomeration and the presence of a regular and homogeneous surface. Thus, the set temperature meets the requirements of the material we want to obtain.

4.2.3. Optical Microscopy Analysis

The influence of organic additives on elaborated membrane textures has been studied (Figure 17) via optical microscopy analysis. The results show a homogeneous surface.

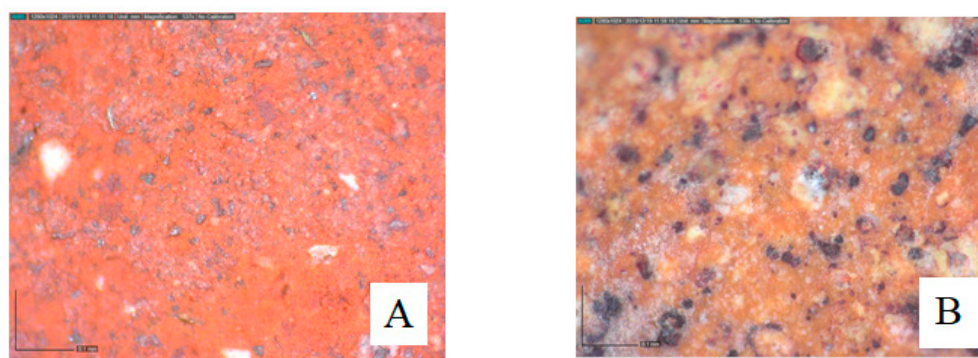


Figure 17. Imaging via optical microscopy of the ferric membrane (A) and clayey membrane (B).

4.2.4. Measurement of Porosity by Nitrogen Adsorption–Desorption Analyses

Nitrogen adsorption–desorption isotherms at 77 K of the ferric membrane, before and after sintering, show isotherms type IV. According to the IUPAC classification [26], these membranes are mesoporous. These isotherms exhibit a type H3 hysteresis (Figures 18 and 19 and Table 4). After sintering, the hysteresis becomes type H4 for clay membranes (Figure 20), suggesting a slit-shaped pore [27].

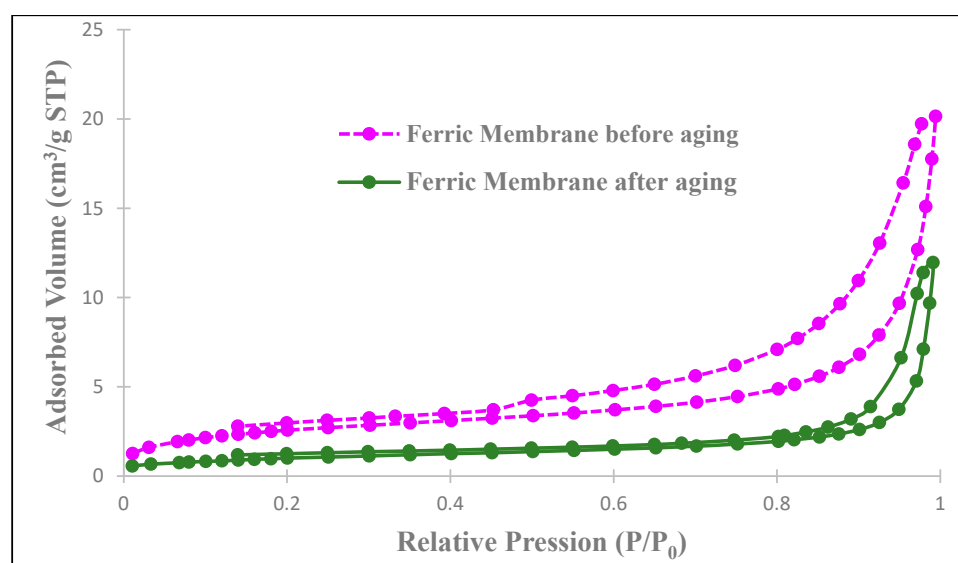


Figure 18. Nitrogen adsorption–desorption isotherm of the two ferric membranes before and after heat treatment.

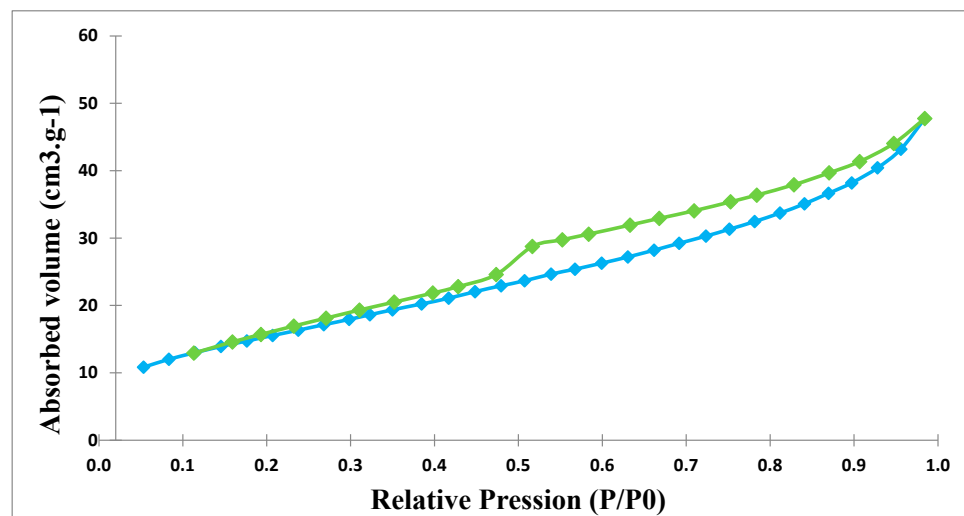


Figure 19. Nitrogen adsorption–desorption isotherm of clay before thermal treatment.

Table 4. Summary of the membranes selected before and after sintering as well as their main textural characteristics: specific surface areas, pore volumes and pore size distributions.

Ferric membrane after firing	S_{BET} ($\text{m}^2 \cdot \text{g}^{-1}$) 3.75	S_{meso}^{BJH} ($\text{m}^2 \cdot \text{g}^{-1}$) 3.17	V_{meso}^{BJH} ($\text{cm}^3 \cdot \text{g}^{-1}$) 0.018	S_{micro} ($\text{m}^2 \cdot \text{g}^{-1}$) 0.51	V_{micro} ($\text{cm}^3 \cdot \text{g}^{-1}$) 0.0001	D (nm) 23.02
Ferric membrane before calcination	S_{BET} ($\text{m}^2 \cdot \text{g}^{-1}$) 9.54	S_{meso}^{BJH} ($\text{m}^2 \cdot \text{g}^{-1}$) 6.98	V_{meso}^{BJH} (cm^2/g) 0.03	S_{micro} ($\text{m}^2 \cdot \text{g}^{-1}$) 0.43	V_{micro} (cm^2/g) 0.00002	D (nm) 17.23
Clay material before calcination	S_{BET} ($\text{m}^2 \cdot \text{g}^{-1}$) 57.69	S_{meso}^{BJH} ($\text{m}^2 \cdot \text{g}^{-1}$) 38.31	V_{meso}^{BJH} (cm^2/g) 0.05	S_{micro} ($\text{m}^2 \cdot \text{g}^{-1}$) 5.48	V_{micro} (cm^2/g) 0.07	D (Å) 19.10
Clayery membrane after calcination	S_{BET} ($\text{m}^2 \cdot \text{g}^{-1}$) 1.75	S_{meso}^{BJH} ($\text{m}^2 \cdot \text{g}^{-1}$) 1.54	V_{meso}^{BJH} (cm^2/g) 0.004	S_{micro} ($\text{m}^2 \cdot \text{g}^{-1}$) 0.16	V_{micro} (cm^2/g) 0.000017	D (nm) 11.79

Specific Surface (S_{BET}), surface and volume of micropores (S_{micro} , V_{micro}), surface and volume of mesopores (S_{meso} , V_{meso}^{BJH}), size of pores via BJH D (nm).

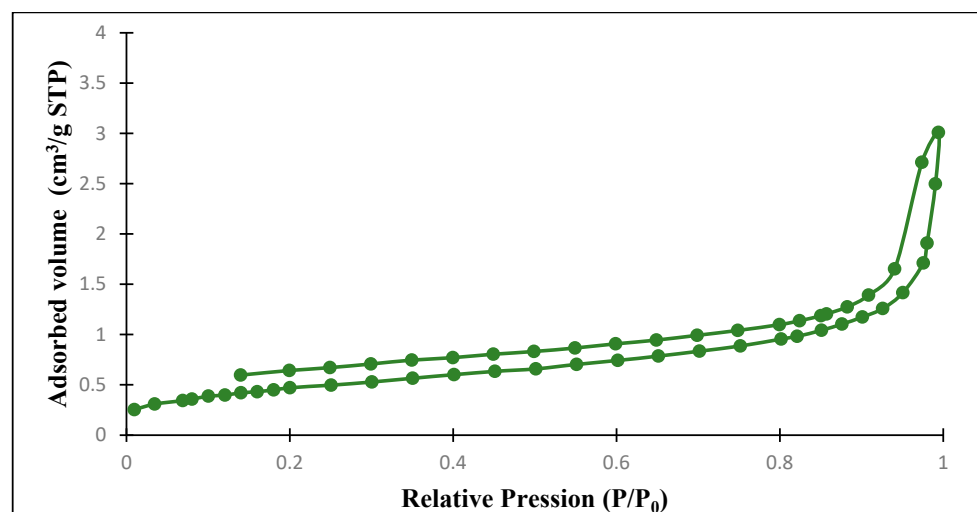


Figure 20. Nitrogen adsorption–desorption isotherm of the clayey membrane after heat treatment.

The enlargement of pores obtained after the firing process and observed in the results summarized in Table 4 describe the Ostwald ripening phenomenon, where small nanoparticles are dissolved and re-deposited onto larger particles. For the Ostwald ripening, the small particles dissolve rapidly. Simultaneously, the larger particles with radius $> r_{\max}$ have growth rates decreasing with r ; thus, their distribution narrows over firing time, leading to the size-focusing.

The heat treatment performed allows the generation of bonds between particles by diffusion of matter [27]. The transport of material is generally carried out by diffusion from convex regions to concave regions, leading to the development and growth of bridges between particles. Diffusion is driven by surface or volume diffusion (Figure 21). The kinetics of all the mechanisms depend on the temperature and the composition (in particular, the impurities). The densification process is present during the treatment carried out, which explains the lowering of the specific surfaces as well as the porous volumes.

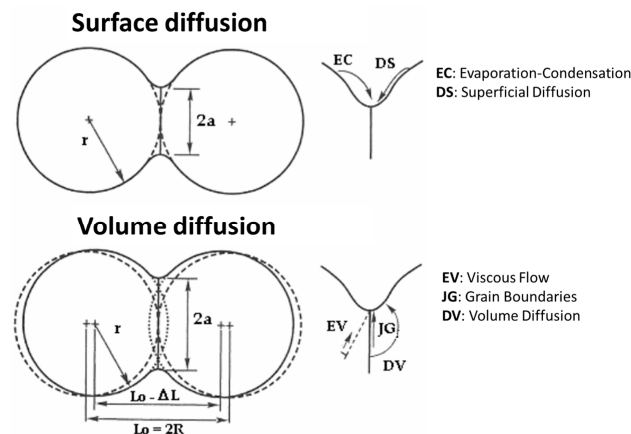


Figure 21. Mechanism of the transport material according to surface diffusion and volume diffusion [28].

Indeed, this process is described by the passage from the assembly of compacted grains of reliable compactness to the creation of trapped pores, often located at the grain boundaries, followed by a significant coarsening of the grain size in the studied sample.

The porosity distribution determined from the N₂ adsorption–desorption isotherms of samples using the BJH method (Figures 22–24) also confirms the material diffusion process. The pore volumes of the two samples show a wide band varying from 5 nm to 40 nm for the ferric membrane and a less important distribution for the clay one, which confirms the data present in the previous adsorption–desorption isotherms and the predominance of mesopores.

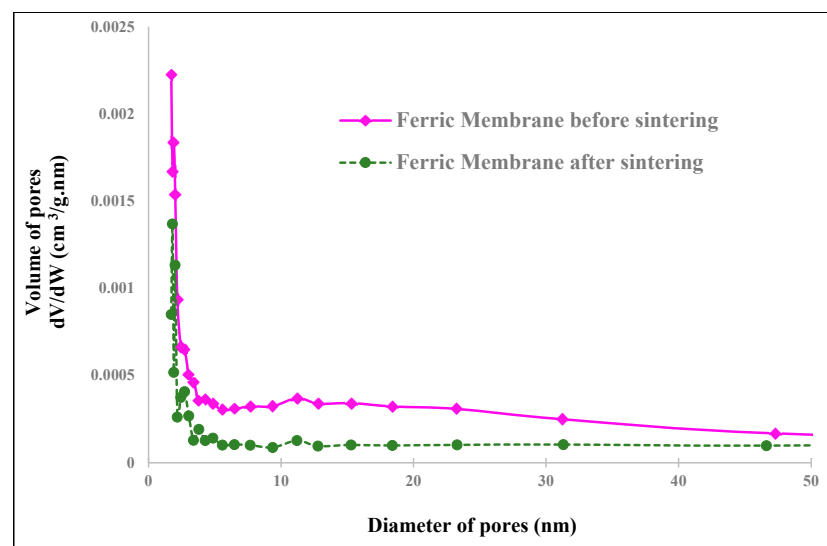


Figure 22. Pore size distribution of ferric membranes (before and after sintering).

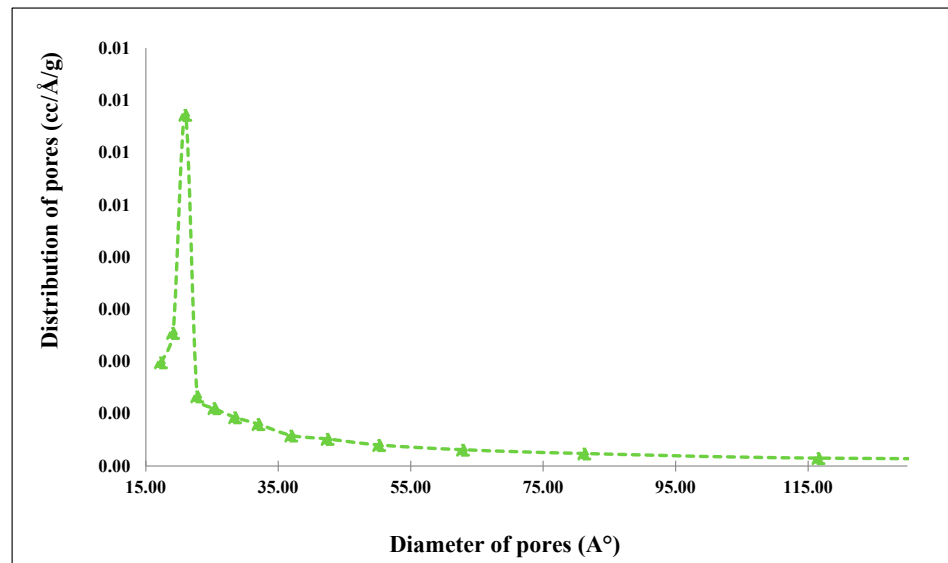


Figure 23. Pore size distribution of raw clay material.

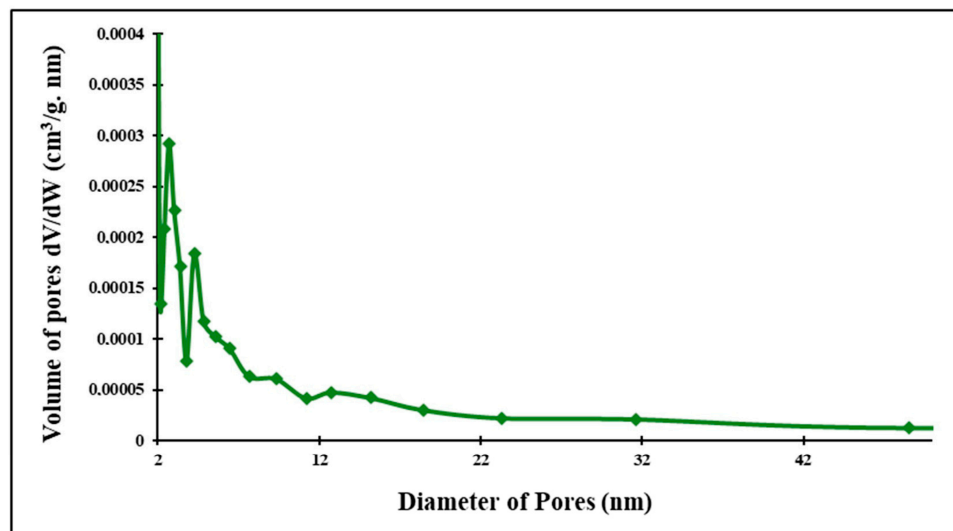


Figure 24. Pore size distribution of clayey membrane after firing.

5. Conclusions

This study focused on the creation of innovative ceramic membranes made from iron and clay. The fabrication process was straightforward, involving the molding of powders into disk sheets. The ideal sintering temperature was determined to be approximately 900 °C, a finding supported by both SEM and optical microscopy, which showed a consistently even surface.

Notably, there was only a minor fluctuation in the rate of mass change (in terms of weight and thickness), measuring at approximately 0.02% with a precision of $\pm 0.001\%$. This observation indicates the stability of the membranes that were synthesized.

The pore distribution in both the ferric and clay-based membranes predominantly exhibits a prevalence of mesopores. The BET isotherms exhibit a type H3 hysteresis. After sintering, the hysteresis became type H4 for clay membranes, suggesting a slit-shaped pore. The pore volume of the two samples shows a wide band varying from 5 nm to 40 nm for the ferric membrane and a less important distribution for the clayey one. Compared to other studies in which local natural material was used to make ceramic membranes, the resulting porosity was among the highest ones reported, which could make application at a larger scale possible.

Ongoing efforts are being made to enhance porosity by incorporating an environmentally friendly pore-forming material. The intention is to subsequently employ these improved materials for gas treatment purposes.

Author Contributions: R.C.: Writing—review and editing. A.C. and S.H., Methodology, Investigation, Project administration. L.M. participated in the characterization of initial materials, F.A.: Supervision, Visualization, Investigation, Writing—review and editing. All authors have read and agreed to the published version of the manuscript.

Funding: This research received no external funding.

Data Availability Statement: The data presented in this study are available on request from the corresponding author.

Acknowledgments: The authors extend their appreciation to the Researchers Supporting Project number (RSP 2023R75), King Saudi University, Riyadh, Saudi Arabia.

Conflicts of Interest: The authors declare that they have no known competing financial interests or personal relationships that could have appeared to influence the work reported in this paper.

References

1. Majouli, A.; Tahiri, S.; Alami Younssi Loukili, S.; Albizane, H.A. Elaboration of new tubular membrane from local Moroccan Perlite for microfiltration process. Application to treatment of industrial wastewaters. *Ceram. Inter.* **2012**, *38*, 4249–4303. [[CrossRef](#)]
2. Palacio, L.; Bouzerdi, Y.; Ouammou, M.; Albizane, A.; Bennazha, J.; Hernandez, A.; Calvo, J.I. Ceramic membranes from morocan naturel clay and phosphate for industrial water treatment. *Desalin* **2009**, *245*, 501–507. [[CrossRef](#)]
3. Hanley, H.J.M. Thermal transpiration measurements on a porous ceramic. *Trans. Faraday Soc.* **1966**, *62*, 2395–2402. [[CrossRef](#)]
4. Boulkrinat, A.; Bouzerara, F.; Harabi, A.; Harrouche, K.; Stelitano, S.; Russo, F.; Galiano, F.; Figoli, A. Synthesis and characterization of ultrafiltration ceramic membranes used in the separation of macromolecular proteins. *J. Eur. Ceram. Soc.* **2020**, *40*, 5967–5973. [[CrossRef](#)]
5. Madaeni, S.S.; Ahmadi Monfared, H.; Vantanpour, V.; Arabi Shamsabadi, A.; Salehi, E.; Daraei, P.; Laki, S.; Khatami, S.M. Coke removal from petrochemical oily wastewater using γ -Al₂O₃ based ceramic microfiltration membrane. *Desalination* **2012**, *293*, 87–93. [[CrossRef](#)]
6. Bouzerara, F.; Harabi, A.; Ghouil, B.; Medjemen, N.; Boudaira, B.; Gondom, S. Elaboration and properties of zirconia microfiltration membrane. *Procedia Eng.* **2012**, *33*, 278–284. [[CrossRef](#)]
7. Qiu, M.; Fan, S.; Gai, Y.; Fan, Y.; Xu, N. Go-sintering synthesis of bi-layer titania ultrafiltration membranes with intermediate layer of sol-coated nanofibers. *J. Membr. Sci.* **2010**, *365*, 225–231. [[CrossRef](#)]
8. Dhivya, A.; Keshav, A. Fabrication of ball clay based low-cost ceramic membrane supports and their characterization for microfiltration application. *J. Indian Chem. Soc.* **2022**, *99*, 100557. [[CrossRef](#)]
9. Eom, J.H.; Yeom, H.J.; Kim, Y.W.; Song, I.H. Ceramic membrane prepared from a silicate and clay-mineral mixture for treatment of oily wastewater. *Clays Clay Miner.* **2015**, *63*, 222–234. [[CrossRef](#)]
10. Hamoudi, L.; Eddine Akretche, D.; Hadadi, A.; Amrane, A.; Mouni, L. Comparative Study of Ceramic Membranes Developed on Different Algerian Natural Clays for Industrial-Effluent Filtration. *Minerals* **2023**, *13*, 273. [[CrossRef](#)]
11. Abbasi, M.; Mirfendereski, M.; Nikbakht, M.M.; Golshenas, T. Mohammadi, Performance study of mullite and mullite-alumina ceramic MF membranes for oily waste waters treatment. *Desalination* **2010**, *259*, 169–178. [[CrossRef](#)]
12. Chihi, R.; Bliidi, I.; Trabelsi-Ayadi, M.; Ayari, F. Elaboration and characterization of a low-cost porous ceramic support from natural Tunisian bentonite clay. *Comptes Rendus Chim.* **2019**, *22*, 188–197. [[CrossRef](#)]
13. Jiang, Q.; Zhou, J.; Miao, Y.; Yang, S.; Zhou, M.; Zhong, Z.; Xing, W. Lower-temperature preparation of SiC ceramic membrane using zeolite residue as sintering aid for oil-in-water separation. *J. Membr. Sci.* **2020**, *610*, 118238. [[CrossRef](#)]
14. Zsrai, T.; Al-Jaml, A.K.; Qiblawey, H.; Al-Marri, M.; Ahmed, A.; Bach, S.; Watson, S.; Judd, S. Ceramic membrane filtration of produced water: Impact of membrane module. *Sep. Purif. Technol.* **2016**, *165*, 214–221. [[CrossRef](#)]
15. Takedo, M.; Onishi, T.; Nakakubo, S.; Fujimoto, S. Physical properties of iron oxide scales on Si-Containing steels at high temperature. *Mater. Trans.* **2009**, *50*, 2242–2246. [[CrossRef](#)]
16. Ross, C.W. Thermal expansion of clay building bricks. *J. Res. Natl. Inst. Stand. Technol.* **1941**, *27*, 197–216. [[CrossRef](#)]
17. Bonekamp, B.C. Chapter 6 Preparation of asymmetric ceramic supports by dip-coating. *Membr. Sci. Technol.* **1996**, *4*, 141–225.
18. Cizeron, G. Le frittage sous son aspect physico-chimique. *Ind. Céramique* **1968**, *154*, 610.
19. Tireli, A.A.; Guimarães, I.R.; Terra, J.C.S.; Da Silva, R.R.; Guerreiro, M.C. Fenton-like processes and adsorption using iron oxide-pillared clay with magnetic properties for ceramic compound mitigation. *Environ. Sci. Pollut. Res.* **2015**, *22*, 870–881. [[CrossRef](#)]
20. Oliveira, L.C.A.; Ramalho, T.C.; Souza, E.F.; Gonçalves, M.; Oliveira, M.C. Catalytic properties of goethite prepared in the presence of Nb on oxidation reactions in water: Computational and experimental studies. *Appl. Catal. B Environ.* **2008**, *83*, 169–176. [[CrossRef](#)]

21. Schwertmann, U.; Cornell, R.M. *Iron Oxides in the laboratory, Preparation and Characterization*; Wiley-VCH: New York, NY, USA, 2008.
22. Chen, Y.H. Thermal properties of nanocrystalline goethite, magnetite, and maghemite. *J. Alloys Compd.* **2013**, *553*, 194–198. [[CrossRef](#)]
23. Rashid, R.Z.A.; Salleh, H.M.; Ani, M.H. Reduction of low-grade iron ore pellet using palm kernel shell. *Renew. Energ.* **2014**, *63*, 617–623. [[CrossRef](#)]
24. Mondal, K.; Lorethova, H.; Hippo, E.; Wiltowski, T.; Lalvani, S.B. Reduction of iron oxide in carbon monoxide atmosphere-reaction controlled kinetics. *Fuel Process. Technol.* **2004**, *86*, 33–47. [[CrossRef](#)]
25. Cornell, R.M.; Schwertmann, U. *The Iron Oxides: Structure, Properties, Reactions, Occurrences and Uses*; WILEY-VCH Verlag GmbH & Co. KGaA: Weinheim, Germany, 2003.
26. Kuczynski, G.C. *Sintering Theory; LA THEORIE DU FRITTAGE*; Technical report, CEA; Centre d'Etudes Nucleaires: Saclay, France, 1960.
27. Sing, K.S. Reporting physisorption data for gas/solid systems with special reference to the determination of surface area and porosity (Recommendations 1984). *Pure Appl. Chem.* **1985**, *57*, 603–619. [[CrossRef](#)]
28. Olmos, L. Etude du Frittage de Poudres par Microtomographie In Situ et Modélisation Discrète. Génie des procédés. Ph.D. Thesis, Institut National Polytechnique de Grenoble—INPG, Grenoble, France, 2009.

Disclaimer/Publisher's Note: The statements, opinions and data contained in all publications are solely those of the individual author(s) and contributor(s) and not of MDPI and/or the editor(s). MDPI and/or the editor(s) disclaim responsibility for any injury to people or property resulting from any ideas, methods, instructions or products referred to in the content.